厚生労働科学研究費補助金

ヒトゲノム・再生医療等研究事業

間葉系幹細胞を用いた移植治療における品質及び安全性判定基準の確立に関する研究

平成 18 年度　総括研究報告書

主任研究者　青山　朋樹

平成 19（2007）年　3 月

目　　次

I.　総括研究報告

間葉系幹細胞を用いた移植治療における品質及び安全性判定基準の確立に関する研究　1

主任研究者　青山朋樹

II.　研究成果の刊行に関する一覧表　2

III. 研究成果の刊行物・別刷

厚生労働科学研究費補助金(ヒトゲノム・再生医療等研究事業)
総括研究報告書

間葉系幹細胞を用いた移植治療における品質及び安全性判定基準の確立に関する研究

主任研究者 青山 朋樹　京都大学再生医科学研究所

研究要旨
間葉系幹細胞はさまざまな組織に分化可能な多能性幹細胞である。このため疾患、外傷などで傷害を受けた組織の修復・再生に期待され、既に臨床応用も開始されている。しかしながら間葉系幹細胞の定義が曖昧であることや施設、技術者によって抽出の方法が異なるなどの理由からその品質を保証する品質管理基準は作成されていない。また*In Vitro*の体外培養において自然発癌例が報告されるなど安全性の監視機構の構築の必要性も高まってきている。
本研究においては品質管理及び安全性監視機構を構築し、臨床試験「難治性骨壊死に対するMSC細胞移植治療」においてその妥当性を検討する。
3年間の間に研究結果を明らかにでき、患者、社会、医療従事者、行政にその情報を還元できる事を特徴としている。

A.研究目的

本研究の目的は間葉系幹細胞(Mesenchymal stem cell, MSC)を用いた細胞医療を行う際の培養(行程あるいは課程)における品質評価及び安全性監視機構を構築することである。

B.研究方法

本研究は平成19年度開始予定の臨床試験「難治性骨壊死に対するMSC細胞移植治療」と連携して実施する。品質評価項目は①MSCの多分化能評価②増殖能評価であり、安全性監視項目は③感染の監視④癌化の監視である。本研究においてはドナー由来のMSCを用いて、これらの4項目を定量的評価し、基準値を作成してそのプロトコールを臨床試験にフィードバックする。臨床試験で得られた問題点を検討し、安全で品質の高い細胞移植治療プロトコールを作成する。

(倫理面への配慮)解析方法の検討に用いるドナー由来のMSCは、京都大学医学部医の倫理委員会の審査を経て実施した。臨床試験は「ヒト幹細胞を用いる臨床研究に関する指針」を遵守しインフォームドコンセントを得られた症例において個人情報の保護・秘匿を遵守して行う予定である。

C.研究結果

品質管理項目である分化能の確認は*In Vitro*で骨、軟骨、脂肪形成能を定量評価する方法を確立し、ドナー由来のMSCで確認済みである。またテロメア長測定、p16遺伝子発現値)が増殖能の予測マーカーとして有効であることが確認できた。

安全性監視項目である感染監視はGMPグレードに準拠したプロトコールを作成し、癌化監視では早期悪性転化のマーカーであるp16遺伝子転写調節領域のメチル化解析が有効であることを発見し、ドナー由来のMSCにおける検討でも有効な結果を得ることができた。

D.考察およびE.結論

平成18年度に作成した品質管理、安全監視のためのプロトコールは確立され、ドナー由来のMSCを用いた検討でも有効であることが実証された。このプロトコールを用いて平成19年度に開始予定の臨床試験「難治性骨壊死に対するMSC細胞移植治療」を開始し、プロトコールの問題点の検討、妥当性を検証していく。

F.健康危険情報

該当なし

G.研究発表

1.論文発表

Shima Y, Aoyama T,et al. In vitro transformation of mesenchymal stem cells by oncogenic H-ras(Val12). Biochem Biophys Res Commun. 2007;353(1):60-66.

2.学会発表

1)嶋靖子、青山朋樹、その他.間葉系幹細胞初代培養系における癌化関連変異の解析第19回日本軟骨代謝学会 2006.3.4 横浜市

2)嶋靖子、青山朋樹、その他.間葉系幹細胞初代培養系における癌化関連遺伝子の変異解析 第39回日本整形外科学会 骨・軟部腫瘍学術集会2006.7.6 札幌市

3)青山朋樹、その他. 間葉系幹細胞移植治療に向けた品質管理機構の構築 第9回日本組織工学会2006.9.8 京都市

4)青山朋樹 間葉系幹細胞の癌化機構とそのモニタリングシステムについての提案 第13回組織工学・再生医学ワークショップ 2006.11.25 大阪市

H.知的財産権の出願・登録状況

「間葉系幹細胞の軟骨細胞分化マーカー」特許申請中

研究成果の刊行に関する一覧表

書籍

該当なし

雑誌

発表者名	論文タイトル名	発表誌名	巻号	ページ	出版年
Ikeguchi R, Aoyama T et al.	Regeneration of osteonecrosis of canine scapho-lunate using bone marrow stromal cells: possible therapeutic approach for Kienbock disease.	Cell Transplant.	15(5)	411	2006
青山朋樹、戸口田淳也.	大腿骨頭壊死の最新治療と再生医学応用の可能性.	治療.	88(11)	2795	2006
Shima Y, Aoyama T et al.	In vitro transformation of mesenchymal stem cells by oncogenic H-ras(Val12).	BBRC	353(1)	60	2007

Cell Transplantation, Vol. 15, pp. 411–422, 2006
Printed in the USA.

0963-6897/06 $90.00 + .00
E-ISSN 1555-3892
www.cognizantcommunication.com

Regeneration of Osteonecrosis of Canine Scapho-lunate Using Bone Marrow Stromal Cells: Possible Therapeutic Approach for Kienböck Disease

Ryosuke Ikeguchi,*†[1] Ryosuke Kakinoki,†[1] Tomoki Aoyama,*[1] Kotaro Roberts Shibata,*† Seiji Otsuka,*§ Kennichi Fukiage,* Koichi Nishijo,*† Tatsuya Ishibe,*† Yasuko Shima,*† Bungo Otsuki,† Takashi Azuma,‡ Sadami Tsutsumi,‡ Tomitaka Nakayama,† Takanobu Otsuka,§ Takashi Nakamura,† and Junya Toguchida*

*Department of Tissue Regeneration, Institute for Frontier Medical Sciences, Kyoto University, Kyoto, Japan
†Department of Orthopaedic Surgery, Graduate School of Medicine, Kyoto University, Kyoto, Japan
‡Department of Medical Simulation Engineering, Institute for Frontier Medical Sciences, Kyoto University, Kyoto, Japan
§Department of Orthopaedic Surgery, Nagoya City University Graduate School of Medical Sciences, Nagoya, Japan

We evaluated the ability of canine bone marrow stromal cells (cBMSCs) to regenerate bone in a cavity of the scapholunate created by curretage and freeze–thawing with liquid nitrogen (LN). Autologous BMSCs were harvested from the iliac crest and expanded in vitro. Their potential to differentiate into osteo-, chondro-, and adipogenic lineages was confirmed using a standard differentiation induction assay. LN-treated scapholunates showed no regeneration of bone tissue when the cavity was left alone, demonstrating severe collapse and deformity as observed in human Kienböck disease. A combination of β-tri-calcium phosphate and a vascularized bone graft with autologous fibroblasts failed to regenerate bone in the LN-treated cavity. When the same procedure was performed using BMSCs, however, LN-treated scapholunates showed no collapse and deformity, and the cavity was completely filled with normal cancerous bone within 4 weeks. These results suggested the potential of using BMSCs to treat Kienböck disease.

Key words: Osteonecrosis; Kienböck disease; Bone marrow stromal cells; Vascularized bone graft; β-Tri-calcium phosphate (β-TCP)

INTRODUCTION

Mesenchymal stem cells (MSCs) represent a stem cell population present in adult tissues that can be isolated, expanded in culture, and characterized in vitro and in vivo. MSCs differentiate readily into chondrocytes, adipocytes, and osteocytes, and can support hematopoietic stem cells or embryonic stem cells in culture (25, 26). The clinical application of MSCs to the regeneration of bone has been investigated in several pathological conditions, including avascular necrosis of bone (1,3, 7,8,10,12,16). In the case of avascular necrosis of the femoral head, favorable clinical results were reported (7,8,12), although direct evidence of the contribution of MSC to the regeneration of bone has yet to be demonstrated.

Kienböck disease (osteonecrosis of the lunate or lunatemalacia) is an avascular necrosis of the lunate (18), of which the precise incidence is unknown. This disease may develop in any individual in the first to eighth decade, but predominantly is found in the dominant hand of male manual worker aged between 20 and 55 years (15). Although its precise etiology is still unknown, poor anatomical vascularity and excess mechanical stress are considered to be important factors related to the occurrence of this disease (15). When the disease becomes advanced, affected lunates will collapse and lose their anatomical structure, which may lead to intercarpal instability, joint incongruity, and osteoarthritic change, resulting in severe pain and disability (28). Because the disease often afflicts young active laborers, treatment should ideally allow the patient to return to work quickly.

A number of surgical procedures have been invented based on two etiological factors mentioned above. Vascularized bone graft (VBG) is the most theoretically reasonable procedure among them because it induces revascularization of and provides mechanical strength to the affected lunate (6,13,17,23,33). However, relatively long-

Received November 1, 2005; final acceptance December 6, 2005.
[1]These three authors contributed equally to this study.
Address correspondence to Junya Toguchida, Institute for Frontier Medical Sciences, Kyoto University, 53 Kawahara-cho, Shogoin, Sakyo-ku, Kyoto 606-8507, Japan. Tel: +81-75-751-4134; Fax: +81-75-751-4646; E-mail: togjun@frontier.kyoto-u.ac.jp

term initial immobilization (up to 3 months) is recommended to prevent the collapse of the lunate, which may limit range of motion (6), and it is known that the lunate after VBG is revascularized slowly and easily recollapses in cases of advanced Kienböck disease (17,23). Ideally, procedures increasing bone strength quickly without affecting wrist function should be combined with VBG to treat advanced Kienböck disease. The transplantation of MSC, with their potential to differentiate into bone-lineage cells, is a promising procedure to accelerate bone regeneration, the effect of which should be investigated in appropriate experimental models. However, there are no ideal animal models of Kienböck disease. Sunagawa et al. reported an experimental model of nonunion with avascular necrosis of the scaphoid using the radial carpal bone (scapholunate) of dogs, in which freeze–thaw treatment was used to inhibit spontaneous healing (30). In this study, we created a severely damaged scapholunate by curretage and freeze–thawing, which showed no spontaneous repair, and investigated the usefulness of MSC transplantation combined with VBG for preventing the collapse of necrotic bone.

MATERIALS AND METHODS

Cell Isolation and Culture

Ten milliliters of bone marrow was aspirated from the iliac crest of a male beagle dog (15 kg) under intravenous anesthesia. The marrow samples were fractionated by centrifugation over a density cushion using Percoll gradient (Amersham Biosciences Corp., Piscataway, NJ) as described previously (4). The interface layer was removed, and nucleated cells were plated on 100-mm culture dishes in DMEM (Sigma Aldrich, St. Louis, MO) supplemented with 10% fetal bovine serum (FBS) (Hyclone, Logan, UT) and antibiotics (0.1 mg/ml of streptomycin and 100 IU of penicillin G), hereafter called the standard medium, at 37°C in a humidified atmosphere of 5% CO_2/95% air. These cells were further cultured as autologous bone marrow stromal cells (BMSCs). Autologous fibroblasts (FBs) were prepared from subcutaneous connective tissue by enzymatic digestion with 0.1% collagenase (Nitta Gelatin, Osaka, Japan). Culture conditions for FBs were the same as for BMSCs. BMSCs and FBs were cultured for 21 days before transplantation, during which the culture medium was changed every other day. Animal experiments were approved by the institutional animal research committee, and performedaccording to the Guidelines for Animal Experiments of Kyoto University.

Induction of Differentiation

Differentiation was induced using the standard method (25), and the content of differentiation induction medium was as described in Table 1. For osteogenic induction, cells (3×10^4) were seeded on six-well plates with standard medium. After 24 h, the medium was replaced with osteogenic induction medium (Table 1), and further cultured for 21 days before the calcification assay. The medium was changed on every other day. For chondrogenic induction, cells (2×10^5) were transferred into a 15-ml polypropylene tube, centrifuged at 1500 rpm for 5 min, and resuspended in 0.5 ml of the chondrogenic induction medium (Table 1). Cells were recentrifuged at the medium change on every other day, and maintained as a small pellet for 21 days. For adipogenic induction, cells (2×10^5) were seeded on six-well plates and cultured with the standard medium. When the cells were confluent, the adipogenic induction was initiated with the induction medium (Table 1) for 3 days and maintained with the maintenance medium (Table 1) for the next 3 days. This cyclic culture was repeated for 21 days.

Transduction of Lentiviral Vector Containing the lacZ Gene

Ampho 293FT cells (6×10^6) (Invitrogen, Carlbad, CA) were seeded on 100-mm culture dishes 24 h before transfection. The lentiviral vector containing the lacZ gene (pLenti-6/V5-GW/lacZ; Invitrogen) was then cotransfected with a mixture of packaging plasmids (pLP1, pLP2, and pLP-VSVG; Invitrogen) by lipofection using lipofectamine 2000 (Invitrogen). The virus-containing supernatant was harvested at 72 h posttransfection and filtered by 0.45 μm filter (Millipore, Billerica, MA). The aliquot was stocked at −80°C before use. For transduction, BMSCs and FBs (1×10^7 each) were seeded on 150-mm culture dishes and incubated with 10 ml of virus-containing supernatant in the presence of polybrene (4 μg/ml). Transduced cells were cultured in DMEM/Ham's F12 with 10% FBS for 24 h before the transplantation.

Reverse Transcription-Polymerase Chain Reaction (RT-PCR)

Total RNA was extracted using Trizol Reagent (Invitrogen), followed by treatment with DNase I (Nippon Gene, Tokyo, Japan). All RT reactions were performed using 1 μg of total RNA with the Super Script First Strand Synthesis System (Invitrogen) according to the manufacturer's instructions. PCR amplification was carried out using 1 μl of RT product in a final volume of 25 μl containing 20 pmol each of the sense and antisense primers, 25 mM $MgCl_2$, 0.2 mM of each dNTP, and one unit of rTaq polymerase (TOYOBO, Osaka, Japan). All PCRs were performed using GeneAmp 9700 (PE Applied Biosystem, Foster City, CA). Sequences of primers are listed in Table 2. PCR products were separated in a 1.5% agarose gel and stained with ethidium bromide. Culture experiments were done at least twice, and the

Table 1. Composition of Differentiation Medium

			Adipogenic Induction	
	Osteogenic Induction	Chondrogenic Induction	Induction Medium	Maintenance Medium
Basic medium	MSC growing medium*	MSC growing medium*	DMEM, high glucose	DMEM, high glucose
Supplements	FBS 10%) Dexamethasone (0.1 mM) Ascorbic acid (50 mM) β-Glycerophosphate (10 mM)	FBS (10%) Dexamethasone (0.1 mM) Ascorbic acid (0.17 mM) Insulin (6.25 mg/ml) Linoleic acid (5.33 mM) Proline (0.35 mM) Selenous acid (6.25 ng/ml) Sodium pyruvate (1 mM) Transferrin (6.25 mg/ml) BSA (1.25 mg/ml) TGF-β3 (0.01 mg/ml)	FBS (10%) Insulin (0.01 mg/ml) Dexamethasone (1 mM) Indomethacin (0.2 mM) 3-Isobutyl-1-methylxanthine (0.5 mM)	FBS (10%) Insulin (0.01 mg/ml)

*Bio Whittaker (Walkersville, MD).

RNA extracted from cells in each experiment was analyzed separately.

Preparation of the Cavity in Scapholunates

In anatomical structure, the canine carpal bone and blood vessels are similar to their human counterparts (34, 35). The experimental model with scapholunate bone was made using a modification of Sunagawa's operation (30). Adult beagle dogs weighing between 15 and 20 kg were used. An IV injection of sodium pentobarbital was used for anesthesia. The scapholunate was exposed dorsally, and a cortical window of 5 × 10 mm was made, through which as much cancerous bone was removed as possible. After the curettage, the cavity was filled with liquid nitrogen (LN) for 10 min, and the frozen bone was thawed at room temperature for 10 min. This

Table 2. Primers Used in the RT-PCR Analyses

Gene	Primers*	Size (bp)	Position	Accession No.
Cbfa1/Runx2	TTCCTGTGCTCTGTGCTGCC GAAACTCTTGCCTCGTCCAC	231	64–83 275–294	AY738265
Alp	ACATACAACACCAACGCTCAG CTTCTCGTCCATCTCATACTC	426	649–669 1054–1074	XM_535374
Osteocalcin	CCTGGAGCCCAAGAGGGAA TGTGGTCAGCCAGCTCGTCAC	62	24–42 65–85	AF2-05942
Col1a1	CTGGAAGAGCGGAGAATACTG GTTGGGTGGGAGGGAGTTTA	609	3880–3900 4469–4488	NM_001003090
Col2a1	ATGGTGGCTTCCACTTCAGC CGATCATAGTCTTGCCCCACTT	291	4081–4100 4350–4371	NM_001006951
Aggrecan	AGGGTTTCGTCCAGCGGCAT TCCTGGAAGCTCCTCTCAGT	176	6842–6861 6998–7017	U65989
Ap2/Fabp4	TGGGTACCTGGAAACTTAGCTC ACGTTTCTGTAATCCGCAGTAAC	226	1928–1949 2131–2153	XM_548843
Ppar-γ	TAAGTCGGATTCACGGATTCG ATAAGGTGGGGATGCAGGCT	298	1287–1307 1565–1584	XM_533738
β-Actin	AAGAGGGGCATCCTGACCCT TACATGGCTGGGGTGTTGAA	218	1645–1664 1843–1862	XM_536888

*All primer sequences are written from 5′ to 3′. For each pair, the top sequence is the sense primer and the bottom sequence is the antisense primer.

freeze–thaw procedure was repeated three times. The same operation was performed on the contralateral side.

Autologous Cell Transplantation

In the treatment groups (five dogs), the cavity was filled with β-tri-calcium phosphate (β-TCP) granules (0.2 cm^2) (Osferion®, Olympus, Tokyo, Japan), and 1×10^7 cells of BMSCs suspended in 500 µl of phosphate-buffered saline (PBS) were carefully injected into the cavity on one side (hereafter called the BM side). The same number of FBs was then injected into opposite side (FB side). Finally the cortical window was plugged with VBG, which was taken from the distal radius and nourished by retrograde blood flow from the 3,4 intercompartmental supraretinacular artery, flowing orthograde into the 2,3 intercompartmental supraretinacular artery and its bony nutrient branch (30). At the time of surgery, bleeding from the cut faces of the bone and arterial pulsation of the pedicle was observed in all VBG.

Imaging Analyses

X-Ray. X-Ray findings were evaluated at 4 weeks after surgery. Antero-posterior and lateral views of both wrists were obtained. The length between the distal capitate and radius was divided by the length of the third metacarpal bone to calculate the carpal height ratio (CHR) from the AP view (38). Ståhl index and angle for radiolunate (RL angle) were measured from the lateral view (9).

Magnetic Resonance Imaging (MRI). MRI was performed on a SIMENS MAGNETOM Sonata1.5 T (40 mT/m maximum amplitude, 200 mT/m/ms slew rate, Germany) with a Flex Coil. The protocol included standard T1-weighted sequence. Details were as follows: repetition time (TR)/echo time (TE), 11.46/5.73 ms; flip angle, 70°; field of view (FOV), 256 × 88 mm; slice thickness, 0.5 mm; bandwidth, 130 Hz/pixel; pixel size, 0.5 × 0.5 mm.

Micro-Computed Tomography (Micro-CT). Canine carpal bones were scanned by CT (SMX-100CT-SV3-type, Shimazu, Kyoto, Japan). The image consisted of 800 slices with a voxel size of 68.224 µm in all three axes. Coronal and sagittal cross-sectional views of the scapholunate were reconstructed using adjunctive software. This same setting was used for all samples. The image reconstruction and quantification of the scapholunate were performed with VG Studio MAX software (Nihon Visual Science, Tokyo, Japan).

Macro- and Microscopic Assessments

The volume and weight of extracted scapholunate bones were calculated. The samples were fixed in a 10% formalin solution at 4°C for 24 h, decalcified with 10% EDTA for 56 days, and then embedded in paraffin. Serial sections were cut at 4 µm and stained with hematoxylin-eosin. Using a light microscope, histological sections were scanned and imported into Adobe Photoshop (Adobe Systems, Mountain View, CA). The bone tissue area for each section was determined by dividing the total number of bone pixels, based on color, by the total area using Image Pro Plus Software (Media Cybernetics, San Diego, CA) (14).

Tartrate-Resistant Acid Phosphate (TRAP) Staining

Deparaffinized sections were washed three times in PBS. Sections were treated with TRAP solution (100 mM sodium acetate, 50 mM sodium tartate, 0.1 mg/ml sodium naphthol AS-MX phosphate, 0.6 mg/ml Fast violet LB, and 0.1% Triton X) at room temperature.

X-gal Staining

The specimens were embedded in Optimum Cutting Temperature (OCT) compound (Sakura Finetechnical Co. Tokyo Japan), and cryosectioned at 6 µm thick. The specimens were postfixed with 4% paraformaldehyde/PBS and rinsed with rinsing buffer (0.1 M $NaHPO_4$, 2 mM $MgCl_2$, 0.01% sodium deoxycholate, and 0.02% Nonidet P-40). The specimens were then incubated overnight at 37°C in the dark in X-gal solution [1 mg/ml of 5-bromo-4-chloro-3-indolyl-β-D-galactopyranoside, 5 mM $K_4Fe(CN)_6$, 5 mM $K_3Fe(CN)_6$, and 20 mM Tris-HCl in rinsing buffer, pH 7.4].

Statistics

Results are expressed as the mean ± SE. The statistical analysis was performed with Student's *t*-test. A significant difference was accepted at the $p < 0.05$ level. Each experimental group was compared with its own control andprepared and analyzed simultaneously.

RESULTS

Potential of cBMSCs to Differentiate

During the growing phase, cBMSCs had a slightly plump, spindle shape, and did not differ greatly from cFBs derived from subcutaneous connective tissues (Fig. 1A, a and b). Transduction efficacy of pLenti-6/V5-GW/lacZ confirmed by X-gal staining was more than 80% in both BMSCs and FBs (data not shown), which remained at least until 4 weeks after transduction (Fig. 1A, c and d). After the osteogenic induction, the expression of the alkaline phosphatase (Alp) and Col1a1 genes was upregulated in cBMSCs but not in cFBs (Fig. 1B). At 21 days after the induction, cBMSCs made a calcified extracellular matrix (ECM) stained with alizarin red and alkaline phosphatase (Fig. 1C). With the adipogenic induction, the expression of adipose tissue-related genes such as the Ap2 and Pparγ genes was upregulated in the cBMSCs

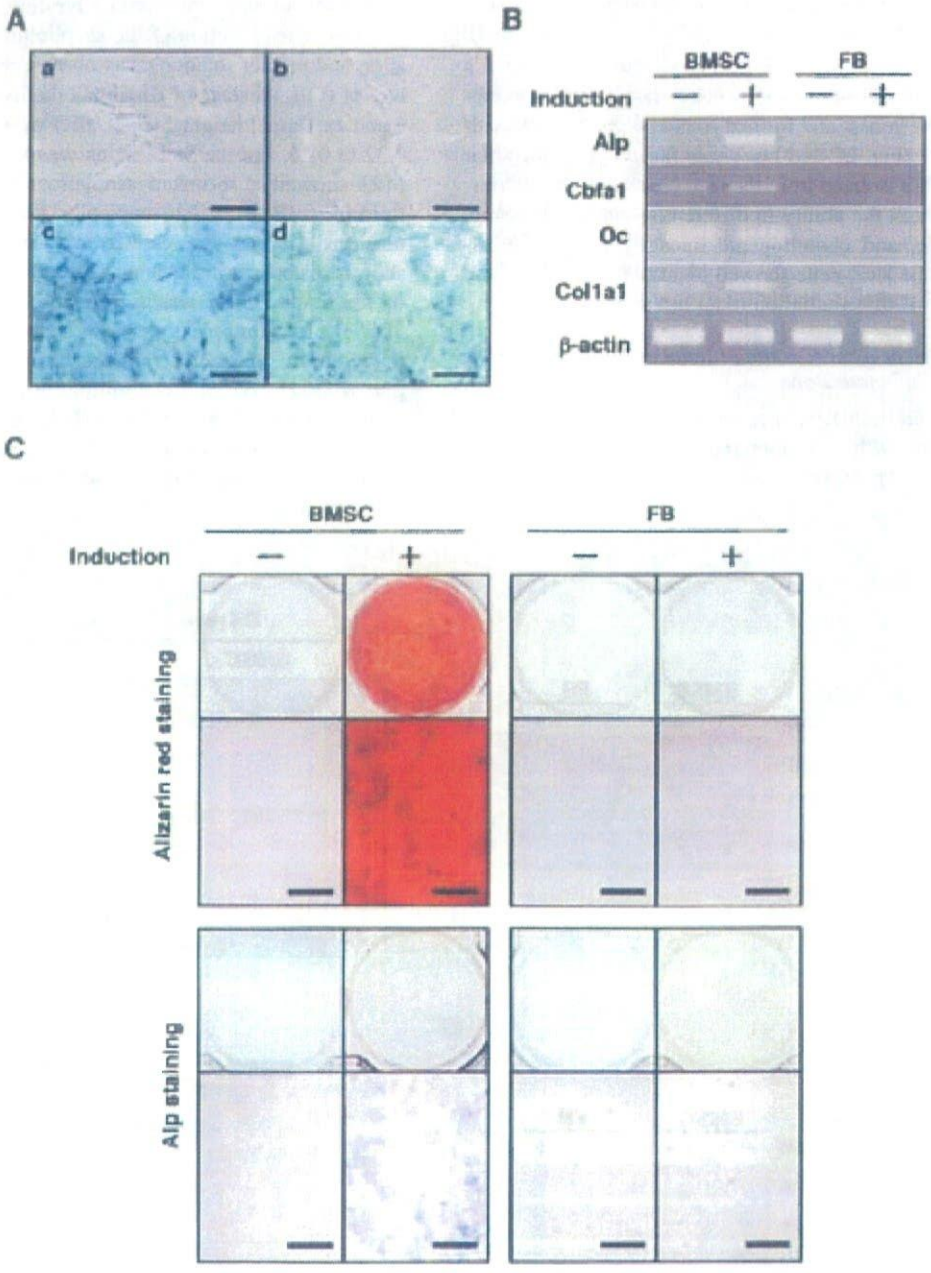

Figure 1. Osteogenic differentiation of cBMSCs. (A) Phase contrast views of BMSCs (a) and FBs (b) in the growing phase. Original magnification: ×100, scale bar: 100 μm. X-gal staining of BMSCs (c) and FBs (d) at 4 weeks after the transduction of pLenti-6/V5-GW/lacZ. Original magnification: ×100, scale bar: 100μm. (B) mRNA expression of bone-related genes in BMSCs and FBs. RNAs were extracted from BMSCs and FBs after 14 days of culture with (+) or without (–) osteogenic induction. (C) Alizarin red and Alp staining of BMSCs and FBs. Cells were cultured with (+) or without (–) osteogenic induction for 14 days and stained. Original magnification: ×40, scale bar: 500 μm.

(Fig. 2A). Intracellular lipid drops stained with Oil red O were abundant in many cBMSCs but not in FBs (Fig. 2B). After a 21-day culture with chondrogenesis cBMSCs expressed cartilage-related genes such as the aggrecan and Col2a1 genes, and formed round pellets stained with alcian blue (Fig. 2C and D). These findings indicated that the cBMSCs isolated from the iliac crest were multipotential cells with the ability to differentiate into osteogenic, adipogenic, and chondrogenic lineages. BMSCs transduced of the lacZ gene showed identical results after the induction of differentiation (data not shown).

LN Treatment After Curettage Induces the Collapse of Scapholunate Bone

In a preliminary experiment, LN-treated scapholunate left alone without any therapeutic intervenion collapsed within 4 weeks (Fig. 3A, c and d). Six months after the operation, the proximal migration of the capitate and rotatory subluxation of the scapholunate (dorsal subluxation and palmer rotation) was observed, which is a feature of the final stage of Kienböck disease (28) (Fig. 3A, e and f). Carpal height ratio (CHR) was decreased from 0.32 to 0.26, and the Ståhl index was from 64% to 40%. MRI showed a shrunken scapholunate surrounded by fluid (Fig. 3B, b). Macroscopically, the radial-side articular cartilage was separated from subchondral bone and showed osteoarthritic change (Fig. 3C, b), and the size of the scapholunate was significantly diminished (Fig. 3D, b). Microscopically, there were trabeculae with many empty lacunae surrounded by necrotic bone marrow (Fig. 3E, a), and a similar finding was observed even in the subchondral area (Fig. 3E, b), indicating that the LN treatment effectively induced osteonecrosis in the scapholunate (Fig. 3E, b). Therefore, there was no

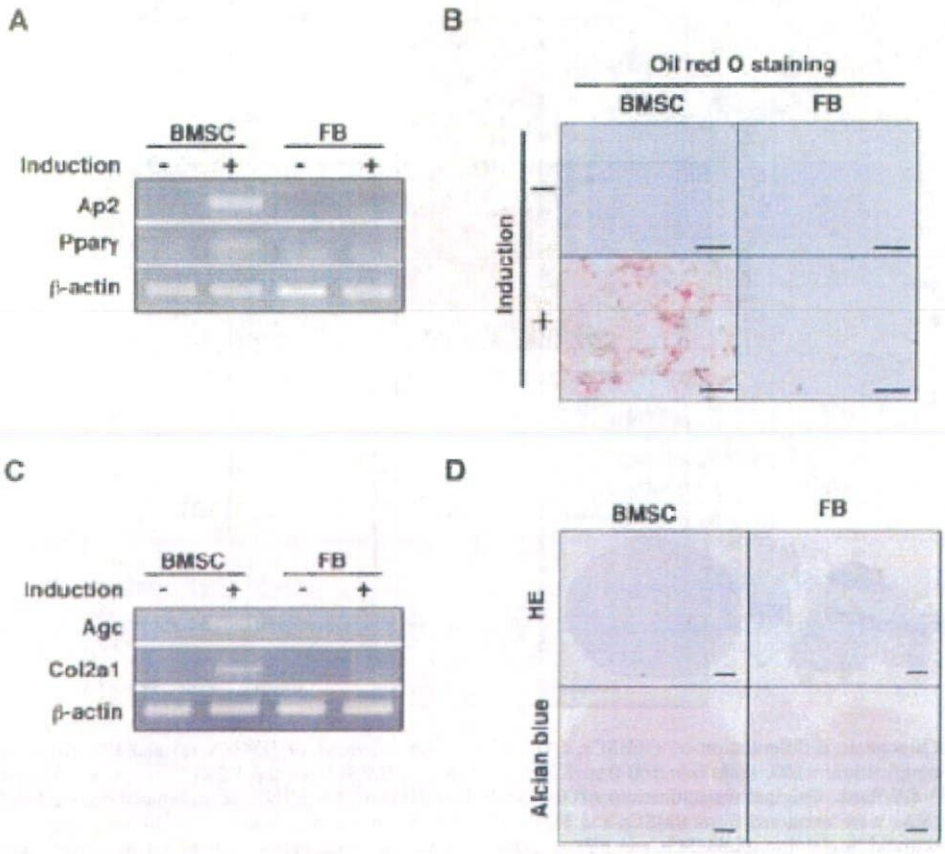

Figure 2. Adipogenic and chondrogenic differentiation of cBMSCs. (A, B) Adipogenic induction of BMSCs and FBs. Cells were culture for 14 days with (+) or without (−) adipogenic induction, and the mRNA expression of adipose tissue-related genes was analyzed by RT-PCR (A), and lipid drop formation was analyzed by Oil red O staining (B). (C, D) Chondrogenic induction of BMSCs and FBs. Cells were cultured as pellets in centrifuge tubes for 14 days, and the mRNA expression of cartilage-related genes was analyzed by RT-PCR (C), and production of proteoglycan was analyzed by alcian blue staining (D). Original magnification: ×200, scale bar: 100μm.

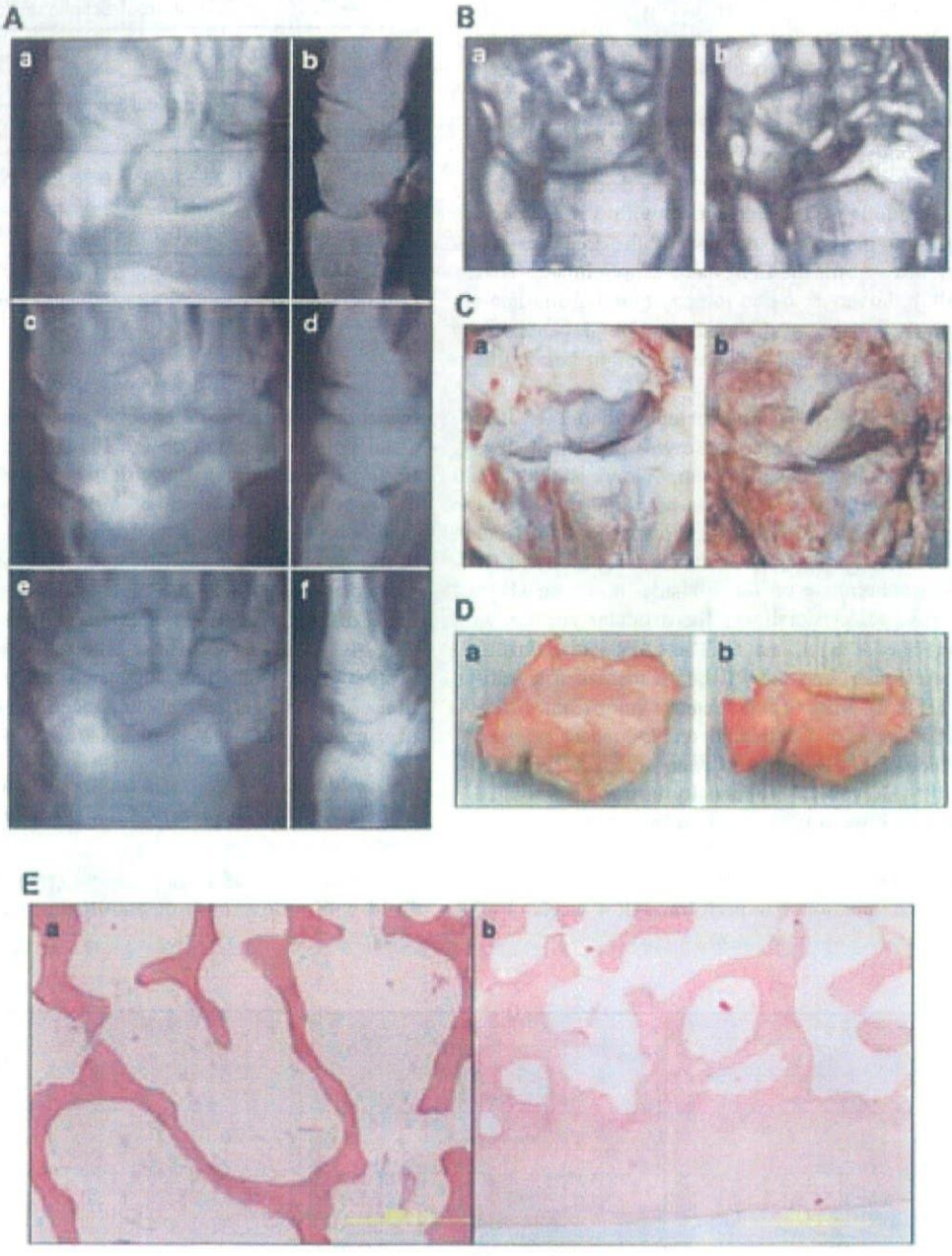

Figure 3. Imaging and morphological changes in LN-treated scapholunate. (A) X-ray findings. AP and lateral view of scapholunate pretreatment (a, b), and at 4 weeks (c, d), and 24 weeks (e, f) posttreatment. Note the proximal migration of the capitate and rotatory subluxation of the scapholunate at 24 weeks posttreatment (e, f). (B) MRI T1-weighted image of MRI before (a) and 24 weeks after (b) the treatment. (C) Macroscopic findings of the radiocapital joint without (a) and with treatment (at 24 weeks) (b). Note the change of color of the joint surface. (D) Macroscopic view of the scapholunate without (a) and with treatment (at 24 weeks) (b). (E) Histological finding of the scapholunate with LN treatment (at 24 weeks) in the periphery of cavity (a) and in the subchondral area (b). Note normal looking articular chondrocytes. Original magnification: ×100, scale bar: 500 μm.

spontaneous healing of the LN-treated scapholunate, suggesting that this model is appropriate for evaluating the effect of therapeutic procedures.

Transplantation of cBMSCs Prevents Collapse of the LN-Treated Scapholunate

As a preliminary experiment, we performed autologous cancerous bone transplantation with VBG, which is our current method of choice for the treatment of Kienböck disease, for the LN-treated scapholunate. This procedure, however, failed to prevent collapse (data not shown): early collapse of the lunate can be prevented by immobilization and the avoidance of weight bearing in human cases.

When cBMSCs were transplanted with β-TCP into the LN-treated cavity, the collapse was prevented (Fig. 4). At 4 weeks after the operation, X-rays showed no collapse on the BM side (Fig. 4A, a, c, and e), and the CHR, Stahl index, and RL angle showed no significant difference from preoperative values (Table 3). LN-treated scapholunate on the FB side, however, showed clear collapse, especially at the articular surface with capitate (Fig. 4A, b, d, and f). The CHR and Stahl indexes were lower, and the RL angle increased significantly (Table 3). MRI also detected a significant difference in the shape of LN-treated scapholunates between the BM side (Fig. 4B, a, c, and e) and FB side (Fig. 4B, b, d, and f). However, the intensity in the T1-weighted image was low in almost the entire scapholunates on both sides (Fig. 4B).

To evaluate the quality of the regenerated tissues, a micro-CT examination was performed at 4 weeks after the operation. Large defects causing a collapse of the distal pole were found on the FB side in all five dogs (Fig. 4C, b, d, and f). Bony tissues in the center of the cavity may be a remnant of VBG, suggesting that no new bone formation was taking place in the LN-treated cavity. In contrast, the LN-treated cavity on the BM side was completely filled with regenerated trabeculae, making it difficult to define the extent of the original cavity (Fig. 4C, a, c, and e). These features were observed in all five dogs. The results suggested that the transplantation of cBMSCs effectively enhanced the reconstruction of cancerous bone tissues in LN-treated scapholunates.

Table 3. X-Ray Evaluation of Scapholunate Bone

Parameters	Preoperative Values	Postoperative Values	
		BM Side	FB Side
CHR	0.32 ± 0.02*	0.31 ± 0.01*	0.28 ± 0.01*
Ståhl index (%)	66 ± 1*	62 ± 3	65 ± 5*
RL angle (degree)	14.7 ± 0.9*	15.7 ± 2.1*	24.3 ± 2.1*

Postoperave values were evaluated at 4 weeks after the operation. CHR was evaluated from the AP view. Ståhl index and RL angle were evaluated from the lateral view.
*$p < 0.05$.

Transplantation of cBMSCs Induces the Absorption of β-TCP by Osteoclasts and Regeneration of Cancerous Bone

Four weeks after the operation, the dogs were sacrificed with an overdose of anesthetic delivered intrave-

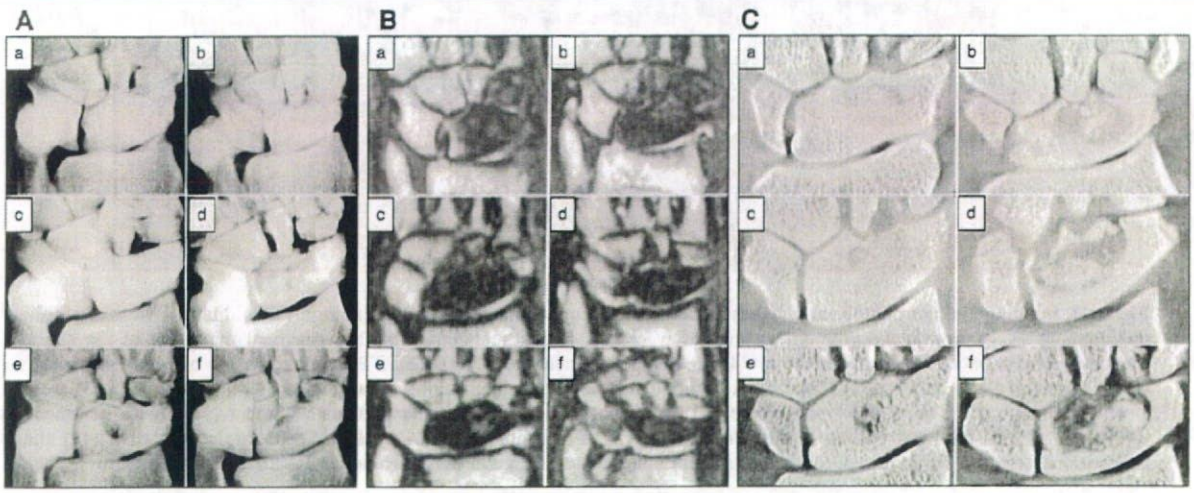

Figure 4. Imaging analyses of LN-treated scapholunate after cell transplantation. Data for three dogs at 4 weeks after the operation are presented. (A) X-ray findings; (B) T1-weighted MRI findings; (C) micro-CT findings. In each analysis, a and b, c and d, and e and f were identical animals, a, c, and e were on the BM side, and b, d, and f were on the FB side.

nously, and LN-treated scapholunates were removed and examined. The volume and weight of LN-treated scapholunates were significantly higher on the BM side than the FB side (Table 4). The bone volume of scapholunate was measured by 3D image reconstruction in each dog, and the value was always larger on the BM than FB side (Table 4). Macroscopically, the cavity of LN-treated scapholunates on the BM side was filled with hard bone-like tissues (Fig. 5A, a), whereas fibrous tissues with an opaque-yellow appearance were found in the corresponding area on the FB side (Fig. 5A, b). The histological findings in the low-power field corresponded with macroscopic appearances; the cavity of the BM side was filled with cancerous bone (Fig. 5B, a), whereas little bone tissue was found in the cavity of the FB side (Fig. 5B, b). Higher magnification showed regenerated trabeculae with normal looking bone marrow and some transition from fibrous tissue to immature bone on the BM side (Fig. 5B, c). Unabsorbed β-TCP granules were occasionally found in trabeculae with a layer of osteoblasts and attached by multinucleated cells (Fig. 5B, e), which were positive for TRAP staining (Fig. 5C, a), suggesting the ongoing resorption of β-TCP by osteoclasts. Completely different features were observed in the specimens taken from the FB side. Most of the cavity was filled with the unabsorbed β-TCP granules with intervening areas of necrotic tissue, and regenerated bone tissue was found only in the peripheral zone with a large amount of unabsorbed β-TCP (Fig. 5B, d). Fibrous tissues were found between the unabsorbed β-TCP, and TRAP-positive multinucleated cells were found adjacent to the β-TCP (Fig. 5C, b), whereas little transition to immature bone tissue was found (Fig. 5B, f). Some osteoblast-like cells lining the surface of the bone structure were positive for X-gal staining, indicating that transplanted cBMSCs participated in the regeneration of bone (Fig. 5D). The area of bone was quantified as described in Materials and Methods. The area of bone was 1.5 times greater on the BM than FB side and the difference was significant (Fig. 5E).

DISCUSSION

The various surgical procedures invented for the treatment of Kienböck disease can be generally classified into three approaches. The first approach is to remove the lunate with or without filling the defect using a tendon or artificial materials (21,22,36). The second approach involves deloading the lunate by joint leveling or intercarpal fusion (5,32,37). The third approach is to revascularize the lunate by using a VBG or vascular pedicle transplantation (13,17,23,33). The VBG is expected to replace the necrotic bone with vascularized osseous tissue and produce new bone around it. However, Moran et al. studied 26 patients with Kienböck disease having undergone VBG to the lunate using magnetic resonance images and revealed that affected lunates were revascularized slowly, and six patients (23%) demonstrated progression of the disease or collapse of the lunate after VBG, leading to osteoarthritic change of the wrist joint (23). Authors reporting excellent clinical outcomes using VBG for the treatment of Kienböck disease combined VBG with other procedures that could deload the lunate, such as long-term cast immobilization of the wrist, joint leveling surgery, or partial carpal fusion (17, 23), which may impede the early rehabilitation and cause a loss of range of motion.

Cell transplantation therapy has already been performed clinically for the aseptic necrosis of the femoral head (7,8,10,12). The initial evidence of the effectiveness of MSCs for the treatment of aseptic necrosis stemmed from an incidental finding, in which bone marrow transplantation for the treatment of sickle cell anemia simultaneously improved steroid-induced aseptic necrosis of the femoral head (10). The same group demonstrated that the MSC pool was decreased in the neck region of the femur with aseptic necrosis of the head (11). Based on these results, they and another group transplanted MSCs directly into the necrotic area after curettage of the necrotic bone, and found that the progression of the disease decreased in the MSC-treated group compared with the control group, although the collapse of the femoral head continued in some cases (7,8,12).

This is the first study to analyze the effect of two therapeutic modalities, VBG and cell transplantation, in large animals with an anatomical structure akin to that of humans. We found that combined therapy effectively and consistently prevented collapse and induced the regeneration of bone in scapholunates with severely damaged remodeling ability. At the initial stage of regeneration, both osteoclasts and osteoblasts exist in the same portion, and a balance between the resorption and formation of bone is required (20). Revascularization takes place surrounding the necrotic bone, which may be the cause of the initial weakening of the regenerating necrotic bone (2). We found multinucleated osteoclasts on both the BM and FB sides (Fig. 5B, C). Multinucleated osteoclasts are produced by the fusion of precursors of

Table 4. Volume and Weight of Scapholunate Bone

Parameters	BM Side	FB Side
Volume (cm^3)	1.58 ± 0.12*	1.43 ± 0.08*
Weight (g)	2.02 ± 0.08*	1.91 ± 0.11*
Bone volume (cm^3)	0.98 ± 0.06*	0.77 ± 0.03*
Bone volume/total volume	0.62 ± 0.08*	0.53 ± 0.03*

Bone volume was evaluated by micro-CT.
*$p < 0.05$.

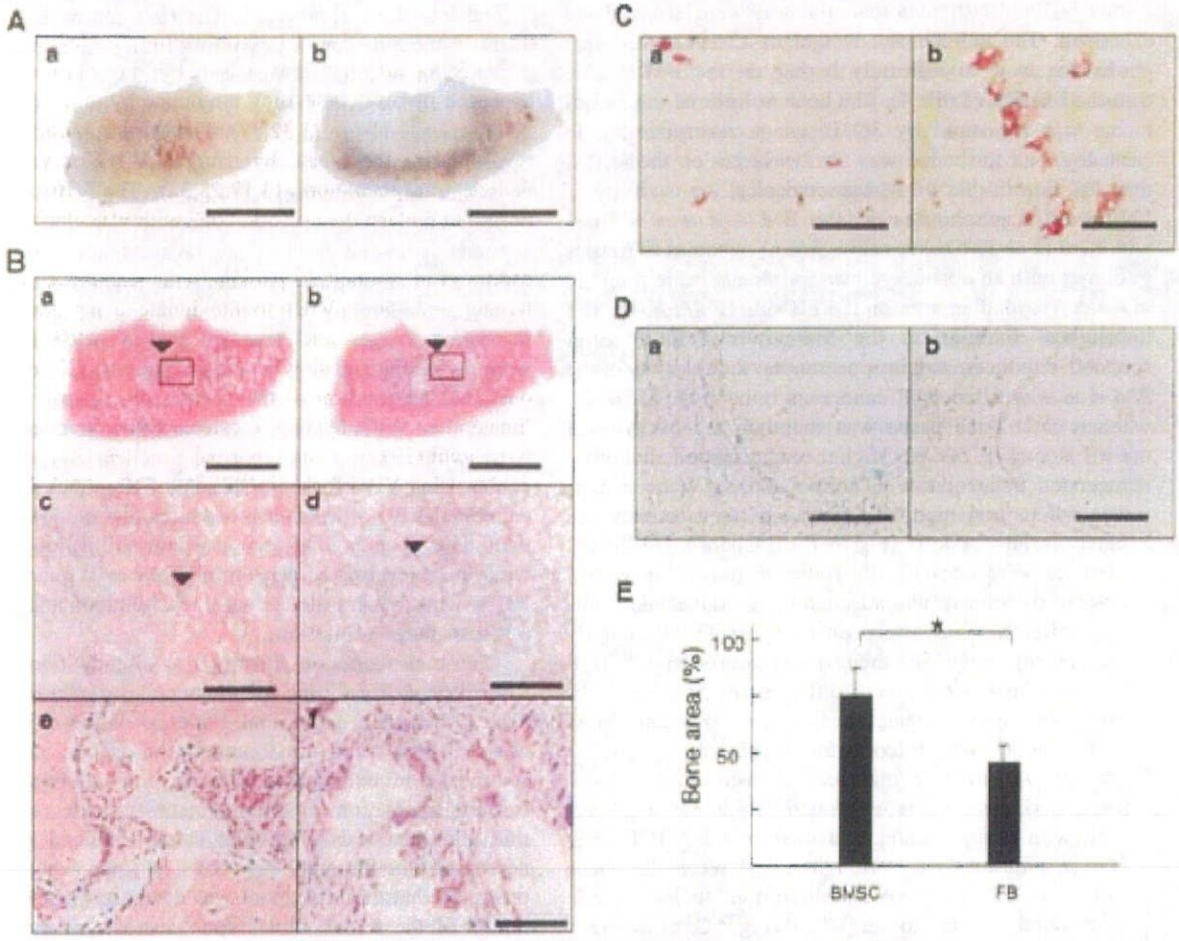

Figure 5. Histological findings of LN-treated scapholunate after cell transplantation. All specimens were from one dog at 4 weeks after the operation. (A) Macroscopic findings of the cut surface of the resected scapholunate on the BM side (a) and FB side (b). (B) HE staining. a, c, and e are scapholunate of the BM side, and b, d, and f are that of the FB side. Original magnification a and b: ×1, scale bar: 1 cm; c and d: ×40, scale bar: 100 μm; e and f: ×400, scale bar: 1 μm. (C) TRAP staining. a, BM side; b, FB side. Original magnification: ×400, scale bar: 100 μM. (D) X-gal staining of the regenerated bone in the BM side. a, X-gal staining; b, negative control. Original magnification: ×400, scale bar: 100 μm. (E) Quantification of bone area. See Materials and Methods. $*p < 0.05$.

hematopoietic and myelomonocytic origin after an appropriate stimulus such as that afforded by RANKL and M-CSF (27). These results suggest that progenitors of osteoclasts were provided via remaining vascular structures and/or VBG equally on both sides. β-TCP is a biodegradable scaffold that has good biocompatibility for the formation of bone (24,31), and is absorbed by activated osteoclasts (19). On the BM side, most of the β-TCP granules seemed to be absorbed, and the rest were surrounded by bone tissues with a layer of osteoblasts on the surface (Fig. 5B, e), which may stimulate multinucleated osteoclasts to absorb β-TCP granules. Although the number of osteoclasts on the FB side was no less than that in the BM side, the resorption of β-TCP was found to be poor on the FB side (Fig. 5B, d and f). Because the activation of osteoclasts requires factors from osteoblasts, the lack of osteoblasts may be the cause of the poor absorption, which may eventually result in poor regeneration of bone tissues. To exclude the possibility that transplantation of fibroblasts inhibits the regeneration of bone, we performed the same operation but with no cell transplantation, and obtained the same result on the FB side (data not shown). Therefore, it is clear that the transplanted BMSCs contributed to the rapid regeneration of bone tissues, although the possibility was not completely excluded that transplanted BMSCs fused with host cells with osteogenic potentials.

We have to admit that our experimental model does

not purely reflect the pathogenesis of Kienböck disease. But it should be noted that the canine scapholunate is a weight-bearing bone and no external or internal immobilization was used after the operation. In spite of this detrimental condition, transplantation of BMSCs prevented early collapse of the necrotic scapholunate consistently, indicating rapid remodeling. The method described here is considered applicable clinically and can be expected to be a powerful tool in the treatment of advanced Kienböck disease, which may help to resolve the clinical problems of VBG. We are currently preparing to start the clinical application performed at the Cell Processing Center in the Kyoto University Hospital.

ACKNOWLEDGMENTS: We thank Drs. Bojian Liang, Yoshiki Kohno, Daisuke Uejima, Moritoshi Furu, and Tomoyuki Yamakawa for their cooperation. This work was supported by Grants-in-aid for Scientific Research from the Japan Society for the Promotion of Science, from the Ministry of Education, Culture, Sports, Science, and Technology, and from the Ministry of Health, Labour, and Welfare.

REFERENCES

1. Arinzeh, T. L.; Peter, S. J.; Archambault, M. P.; van den Bos, C.; Gordon, S.; Kraus, K.; Smith, A.; Kadiyala, S. Allogeneic mesenchymal stem cells regenerate bone in a critical-sized canine segmental defect. J. Bone Joint Surg. Am. 85:1927–1935; 2003.
2. Aspenberg, P.; Wang, J. S.; Jonsson, K.; Hagert, C. G. Experimental osteonecrosis of the lunate. Revascularization may cause collapse. J. Hand Surg. Br. 19:565–569; 1994.
3. Bruder, S. P.; Kraus, K. H.; Goldberg, V. M.; Kadiyala, S. The effect of implants loaded with autologous mesenchymal stem cells on the healing of canine segmental bone defects. J. Bone Joint Surg. Am. 80:985–996; 1998.
4. Caterson, E. J.; Nesti, L. J.; Danielson, K. G.; Tuan, R. S. Human marrow-derived mesenchymal progenitor cells: isolation, culture expansion, and analysis of differentiation. Mol. Biotechnol. 20:245–256; 2002.
5. De Smet, L.; Verellen, K.; D'Hoore, K.; Buellens, C.; Lysens, R.; Fabry, G. Long-term results of radial shortening for Kienböck's disease. Acta Orthop. Belg. 61:212–217; 1995.
6. Gabl, M.; Lutz, M.; Reinhart, C.; Zimmerman, R.; Pechlaner, S.; Hussl, H.; Rieger, M. Stage 3 Kienböck's disease: Reconstruction of the fractured lunate using a free vascularized iliac bone graft and external fixation. J. Hand Surg. Br. 27:369–373; 2002.
7. Gangji, V.; Hauzeur, J. P.; Matos, C.; De Maertelaer, V.; Toungouz, M.; Lambermont, M. Treatment of osteonecrosis of the femoral head with implantation of autologous bone-marrow cells. A pilot study. J. Bone Joint Surg. Am. 86:1153–1160; 2004.
8. Gangji, V.; Hauzeur, J. P. Treatment of osteonecrosis of the femoral head with implantation of autologous bone-marrow cells. J. Bone Joint Surg. Am. 87:106–112; 2005.
9. Goldfarb, C. A.; Hsu, J.; Gelberman, R. H.; Boyer, M. I. The Lichtman classification for Kienböck's disease: An assessment of reliability. J. Hand Surg. Am. 28:74–80; 2003.
10. Hernigou, P.; Bernaudin, F.; Reinert, P.; Kuentz, M.; Vernant, J. P. Bone-marrow transplantation in sickle-cell disease. Effect on osteonecrosis: A case report with a four-year follow-up. J. Bone Joint Surg. Am. 79:1726–1730; 1997.
11. Hernigou, P.; Beaujean, F.; Lambotte, J. C. Decrease in the mesenchymal stem-cell pool in the proximal femur in corticosteroid-induced osteonecrosis. J. Bone Joint Surg. Br. 81:349–355; 1999.
12. Hernigou, P.; Beaujean, F. Treatment of osteonecrosis with autologous bone marrow grafting. Clin. Orthop. Relat. Res. 405:14–23; 2002.
13. Hori, Y.; Tamai, S.; Okuda, H.; Sakamoto, H.; Takita, T.; Masuhara, K. Blood vessel transplantation to bone. J. Hand Surg. Am. 4:23–33; 1979.
14. Huang, Y. C.; Kaigler, D.; Rice, K. G.; Krebsbach, P. H.; Mooney, D. J. Combined angiogenic and osteogenic factor delivery enhances bone marrow stromal cell-driven bone regeneration. J. Bone Miner. Res. 20:848–857; 2005.
15. Irisarri, C. Aetiology of Kienböck's disease. J. Hand Surg. Br. 29:281–287; 2004.
16. Kadiyala, S.; Young, R. G.; Thiede, M. A.; Bruder, S. P. Culture expanded canine mesenchymal stem cells possess osteochondrogenic potential in vivo and in vitro. Cell Transplant. 6:125–134; 1997.
17. Kakinoki, R.; Matsumoto, T.; Suzuki, T.; Funakoshi, N.; Okamoto, T.; Nakamura, T. Lunate plasty for Kieböck's disease: Use of a pedicled vascularised radial bone graft combined with shortening of the capitate and radius. Hand Surg. 6:145–156; 2001.
18. Kienböck, R. Uber traumatische Malazie des Mondbeins und ihre Folgezustande. Fortshritte auf dem Gebiete der Roentgenstrahlen 16:78–103; 1910.
19. Kondo, N.; Ogose, A.; Tokunaga, K.; Ito, T.; Arai, K.; Kudo, N.; Inoue, H.; Irie, H.; Endo, N. Bone formation and resorption of highly purified beta-tricalcium phosphate in the rat femoral condyle. Biomaterials 26:5600–5608; 2005.
20. Li, M.; Amizuka, N.; Oda, K.; Tokunaga, K.; Ito, T.; Takeuchi, K.; Takagi, R.; Maeda, T. Histochemical evidence of the initial chondrogenesis and osteogenesis in the periosteum of a rib fractured model: Implications of osteocyte involvement in periosteal chondrogenesis. Microsc. Res. Tech. 64:330–342; 2004.
21. Lichtman, D. M.; Mack, G. R.; MacDonald, R. I.; Gunther, S. F.; Wilson, J. N. Kienböck's disease: The role of silicone replacement arthroplasty. J. Bone Joint Surg. Am. 59:899–908; 1977.
22. Lichtman, D. M.; Alexander, A. H.; Mack, G. R.; Gunther, S. F. Kienböck's disease—update on silicone replacement arthroplasty. J. Hand Surg. Am. 7:343–347; 1982.
23. Moran, S. L.; Cooney, W. P.; Berger, R. A.; Bishop, A. T.; Shin, A. Y. The use of the 4 + 5 extensor compartmental vascularized bone graft for the treatment of Kienböck's disease. J. Hand Surg. Am. 30:50–58; 2005.
24. Ohsawa, K.; Neo, M.; Matsuoka, H.; Akiyama, H.; Ito, H.; Kohno, H.; Nakamura, T. The expression of bone matrix protein mRNAs around beta-TCP particles implanted into bone. J. Biomed. Mater. Res. 52:460–466; 2000.
25. Pittenger, M. F.; Mackay, A. M.; Beck, S. C.; Jaiswal, R. K.; Douglas, R.; Mosca, J. D.; Moorman, M. A.; Simonetti, D. W.; Craig, S.; Marshak, D. R. Multilineage potential of adult human mesenchymal stem cells. Science 284:143–147; 1999.
26. Pittenger, M. F.; Martin, B. J. Mesenchymal stem cells and their potential as cardiac therapeutics. Circ. Res. 95: 9–20; 2004.

27. Quinn, J. M.; Gillespie, M. T. Modulation of osteoclast formation. Biochem. Biophys. Res. Commun. 328:739–745; 2005.
28. Salmon, J.; Stanley, J. K.; Trail, I. A. Kienböck's disease: Conservative 23 management versus radial shortening. J. Bone Joint Surg. Br. 82:820–823; 2000.
29. Schmitt, R.; Heinze, A.; Fellner, F.; Obletter, N.; Struhn, R.; Bautz, W. Imaging and staging of avascular osteonecroses at the wrist and hand. Eur. J. Radiol. 25:92–103; 1997.
30. Sunagawa, T.; Bishop, A. T.; Muramatsu, K. Role of conventional and vascularized bone grafts in scaphoid nonunion with avascular necrosis: A canine experimental study. J. Hand Surg. Am. 25:849–859; 2000.
31. Takahashi, Y.; Yamamoto, M.; Tabata, Y. Osteogenic differentiation of mesenchymal stem cells in biodegradable sponges composed of gelatin and beta-tricalcium phosphate. Biomaterials 26:3587–3596; 2005.
32. Takase, K.; Imakiire, A. Lunate excision, capitate osteotomy, and intercarpal arthrodesis for advanced Kienböck disease. Long-term follow-up. J. Bone Joint Surg. Am. 83: 177–183; 2001.
33. Tamai, S.; Yajima, H.; Ono, H. Revascularization procedures in the treatment of Kienböck's disease. Hand Clin. 9:455–466; 1993.
34. Tu, Y. K.; Bishop, A. T.; Kato, T.; Adams, M. L.; Wood, M. B. Experimental carpal reverse-flow pedicle vascularized bone grafts. Part I: The anatomical basis of vascularized pedicle bone grafts based on the canine distal radius and ulna. J. Hand Surg. Am. 25:34–45; 2000.
35. Tu, Y. K.; Bishop, A. T.; Kato, T.; Adams, M. L.; Wood, M. B. Experimental carpal reverse-flow pedicle vascularized bone grafts. Part II: Bone blood flow 24 measurement by radioactive-labeled microspheres in a canine model. J. Hand Surg. Am. 25:46–54; 2000.
36. Ueba, Y.; Nosaka, K.; Seto, Y.; Ikeda, N.; Nakamura, T. An operative procedure for advanced Kienböck's disease. Excision of the lunate and subsequent replacement with a tendon-ball implant. J. Orthop. Sci. 4:207–215; 1999.
37. Weiss, A. P.; Weiland, A. J.; Moore, J. R.; Wilgis, E. F. Radial shortening for Kienböck disease. J. Bone Joint Surg. Am. 73:384–391; 1991.
38. Youm, Y.; McMurthy, R. Y.; Flatt, A. E.; Gillespie, T. E. Kinematics of the wrist. I. An experimental study of radial-ulnar deviation and flexion-extension. J. Bone Joint Surg. Am. 60:423–431; 1978.

Available online at www.sciencedirect.com
ScienceDirect
Biochemical and Biophysical Research Communications 353 (2007) 60–66
BBRC
www.elsevier.com/locate/ybbrc

In vitro transformation of mesenchymal stem cells by oncogenic H-*ras*^{Val12}

Yasuko Shima [a,b], Takeshi Okamoto [a,b], Tomoki Aoyama [a], Ko Yasura [a], Tatsuya Ishibe [a,b], Koichi Nishijo [a,b], Kotaro R. Shibata [a,b], Yoshiki Kohno [a,b], Kenichi Fukiage [a], Seiji Otsuka [a,c], Daisuke Uejima [a,d], Tomitaka Nakayama [b], Takashi Nakamura [b], Tohru Kiyono [e], Junya Toguchida [a,*]

[a] *Institute for Frontier Medical Sciences, Kyoto University, 53 Kawahara-cho, Shogoin, Sakyo-ku, Kyoto 606-8507, Japan*
[b] *Department of Orthopaedic Surgery, Graduate School of Medicine, Kyoto University, Kyoto, Japan*
[c] *Department of Musculoskeletal Medicine, Graduate School of Medical Sciences, Nagoya City University, Nagoya, Japan*
[d] *Department of Orthopaedic Surgery, Kansai Medical University, Moriguchi, Japan*
[e] *Virology Division, National Cancer Center Research Institute, Tokyo, Japan*

Received 17 November 2006
Available online 6 December 2006

Abstract

Tissue stem cells may serve as progenitors for malignant tumors derived from the same tissue. Here, we report the establishment of immortalized human mesenchymal stem cells (ihMSC) and tested the feasibility of using ihMSC as presarcomatous cells. Immortalization was achieved by introducing the genes for human telomerase reverse transcriptase and Bmi1. ihMSC retained the potential for multidirectional differentiation of the original MSC. To transform ihMSC, we introduced an oncogenic H-*ras*^{Val12} gene, and established the cell line ihMSC-*ras*. ihMSC-*ras* had the phenotype of fully transformed cells and retained adipogenic and chondrogenic, but not osteogenic, potential. Interestingly, ihMSC-*ras* demonstrated morphological features of autophagy, and inhibition of the ERK pathway suppressed the production of autophagosomes, indicating that ras/ERK signaling is responsible for the induction of autophagy. Thus ihMSC will serve as a material with which to analyze the tumorigenic and differentiation-modifying effects of candidate oncogenes involved in the development of sarcomas.

Keywords: Mesenchymal stem cell; TERT; Bmi1; *ras*; Transformation; Autophagy; Differentiation

Sarcomas are defined as malignant tumors derived from non-epithelial tissues, but the precursors of sarcoma cells are equivocal in most cases. For example, osteosarcomas, the most common malignant bone tumor, are defined as tumors producing immature bone tissue called osteoid. This definition, however, does not mean that the precursors of osteosarcomas are cells committed to the osteoblastic lineage. One major histological subtype of osteosarcoma is the chondroblastic osteosarcoma, in which cartilaginous tissues are formed directly by tumor cells expressing a number of cartilage-related genes [1], suggesting that cells of this type of osteosarcoma have the potential to differentiate in at least two directions. Most osteosarcomas develop from bone marrow, and therefore bone marrow stromal cells are reasonable candidates for the precursors of osteosarcomas, and the most plausible candidate cells are mesenchymal stem cells (MSCs). MSCs are defined as cells with the potential to differentiate into a variety of mesenchymal cell lineages [2], and therefore have the potential to be the precursor of a variety of mesenchymal tumors, although there have been no reports showing the development of a particular type of sarcoma from MSC. Considering that transformation requires the immortalization step, immortalized

* Corresponding author. Fax: +81 75 751 4144.
E-mail address: togjun@frontier.kyoto-u.ac.jp (J. Toguchida).

0006-291X/$ - see front matter © 2006 Elsevier Inc. All rights reserved.
doi:10.1016/j.bbrc.2006.11.137

human MSC as presarcomatous cells would be a suitable material with which to test the oncogenic potential of candidate genes.

In this study, we tried to immortalize hMSC by inactivating the $p16^{INK4A}$ gene using the Bmi1 gene. Bmi1 was first identified as an oncogene that cooperates with c-myc in the generation of mouse lymphomas [3]. Bmi1 is a nuclear protein which makes a complex with other polycomb group proteins and binds to polycomb response elements to inhibit the transcription of target genes including the $p16^{INK4A}$ gene [4]. A recent report stated that Bmi1 is required for the self-renewal of stem cells in the peripheral and central nervous systems [5]. The Bmi1 gene is also thought to regulate the replicative life span of human fibroblasts [6] and recent reports described the immortalization of human ovarian surface epithelial cells [7] and mesenchymal stem cells [8].

Here, we established immortalized human MSC (ihMSC), which retained the potential for multi-directional differentiation of the original cells, and tested the feasibility of using ihMSC as presarcomatous cells.

Materials and methods

Cell culture and reagents. Adult hMSC were purchased from Bio Whittaker, and cultured in MSC growing medium (Bio Whittaker). EJ and Saos2 were obtained from American Type Culture Collection, and Ampho293 was obtained from Clontech and cultured in Dulbecco's Modified Eagle's medium (DMEM, Sigma–Aldrich) with 10% fetal bovine serum (FBS, Hyclone).

Antibodies against phospho-p44/42 MAPK (p-ERK1/2), pan-ERK, phospho-p38 (p-p38), pan-p38, and $p16^{INK4A}$ were purchased from BD Biosciences. The antibody against human LC3 [9] was kindly provided by Dr. Mizushima (National Institute for Basic Biology, Japan). The MEK inhibitor U0126 was obtained from Promega.

Reverse transcription (RT)-PCR. Total RNA was extracted from cells and pellets using an RNAse Easy Mini Kit (Qiagen), and reverse-transcribed with the Superscript III first strand system (Invitrogen). The synthesized cDNA was used as a template for each PCR, and the products were electrophoresed on 1.5–2% agarose gels and visualized by ethidium bromide staining. Information on the primer pairs used in the RT-PCR is available upon request.

Retroviral vectors and infections. Retroviral vectors expressing hTERT and the Bmi1 gene were previously described [10]. A retroviral vector expressing oncogenic H-ras^{Val12} was constructed using RNA derived from the bladder carcinoma cell line EJ, which contained an oncogenic H-ras^{Val12} gene [11]. After the reverse transcription, the entire coding region of the H-ras^{Val12} gene was amplified and first cloned into a TA vector (Invitrogen), plasmids containing the correct sequence were selected, and the subcloned into a retroviral vector pQCXIP-IRES-PURO (Clontech).

Amphotropic retroviruses were produced by transfection of the ampho293 producer cell lines with each retroviral vector using lipofectamine 2000 (Invitrogen). Cells were infected with amphotropic retroviruses in 6 μg/ml of polybrane, and purified by selection with 100 μg/ml of hygromycin B (Sigma–Aldrich) or 100 μg/ml of G418 (Sigma–Aldrich).

Western blotting. SDS-sample buffer was added directly to the dishes, and cells were stripped with a cell scraper, and the cell lysate was then sonicated. Total protein (20 μg) was electrophoresed on SDS polyacrylamide gels and transferred to Immobilon-P membranes (Millipore). The membranes were blocked using a 5% dried milk powder, and incubated with the antibody against each protein. They were then washed and incubated with horseradish peroxidase (HRP)-conjugated goat anti-mouse IgG (Santa Cruz Biotechnology) and HRP-conjugated swine anti rabbit IgG (DAKO) and detected using enhanced chemiluminescence plus reagents (Amersham Pharmacia Biotech).

Northern blot analysis. Total RNA was isolated from cells using Sepasol reagent (Nacalai tesque). Ten micrograms of total RNA was separated on a 1% agarose–formaldehyde gel, and blotted on to a nylon membrane, and hybridized with ^{32}P-labeled probes. A part of the cDNA of the human H-*ras* gene (NM005343) was amplified by RT-PCR and used as a probe.

Telomere length and telomerase assay. Telomere length was measured as described previously [12]. The telomerase activity in cells was detected with the telomeric repeat amplification protocol (TRAP) as described previously [12] using a Telo Chaser Kit (Toyobo).

Transmission electron microscopy. Cells were fixed with ice-cold 2% glutaraldehyde in 0.1 M cacodylate buffer (pH 7.0), and thin sections (70–80 nm) were prepared and stained with uranyl acetate and lead citrate and observed using a transmission electron microscope.

G-banding karyotypic analysis. Metaphase spreads were prepared from cells treated with colcemid, and 50 metaphases were analyzed by the standard G-banding method.

Phenotype analyses

Proliferation assay. Cells (1×10^4) were seeded in 60-mm culture dishes in triplicate, and cultured in DMEM with 1% or 10% FBS. The number of cells in each dish was counted by hemocytometer at each time point.

Soft agar assay. Cells (1×10^4) were suspended in 0.35% low-melting point agarose dissolved in DMEM with 10% FBS, and seeded in 60-mm culture dishes precoated with 0.7% agarose. After 2 weeks, colonies in three random fields of view at 200× magnification were scored. Experiments were performed in triplicate.

Matrigel invasion assay. Cell suspensions (2.5×10^4/0.5 ml DMEM) were added into the upper wells of 24-well chambers (BD Biosciences). After incubation for 22 h, invading cells were fixed with 100% methanol and stained with 1% Toluidine blue. Cells in five random fields of view at 200× magnification were counted and expressed as the average number of cells per field of view. Data were expressed as the percent invasion through the matrigel membrane relative to the migration through the control membrane.

In vivo tumor formation. Cell suspensions containing 5×10^6 cells in 100 μl of PBS were injected subcutaneously into immunodeficient mice (BALB/c nu/nu). Three mice were used for each cell type. Tumor volume was calculated with the formula $4/3\pi r^3$.

Differentiation assay. Adipogenic, osteogenic, and chondrogenic differentiation were performed as previously described [12], and Oil-Red-O staining, Alizarin red staining, and Alcian blue staining were used to evaluate the differentiation as previously described [12].

Results

Establishment of Bmi1-hTERT-immortalized hMSC

After the sequential introduction of the hTERT and Bmi1 genes into hMSC, drug-resistant cells were selected and propagated. This polyclonal cell line, designated hMSC-Bmi1-hT, grew much faster than the original hMSC with a doubling time of 48 h, and showed no signs of entering senescence after more than 24 months. The telomerase activity of hMSC-Bmi1-hT was comparable with that of Hela (Fig. 1A), and the telomere length was maintained even in late passaged cells (Fig. 1B). Expression of the exogenous Bmi1 gene was confirmed by Northern blotting (Fig. 1C), and the expression of the $p16^{INK4A}$ gene was markedly downregulated at both the mRNA and protein level (Fig. 1D). This immortalized line may consist of cells

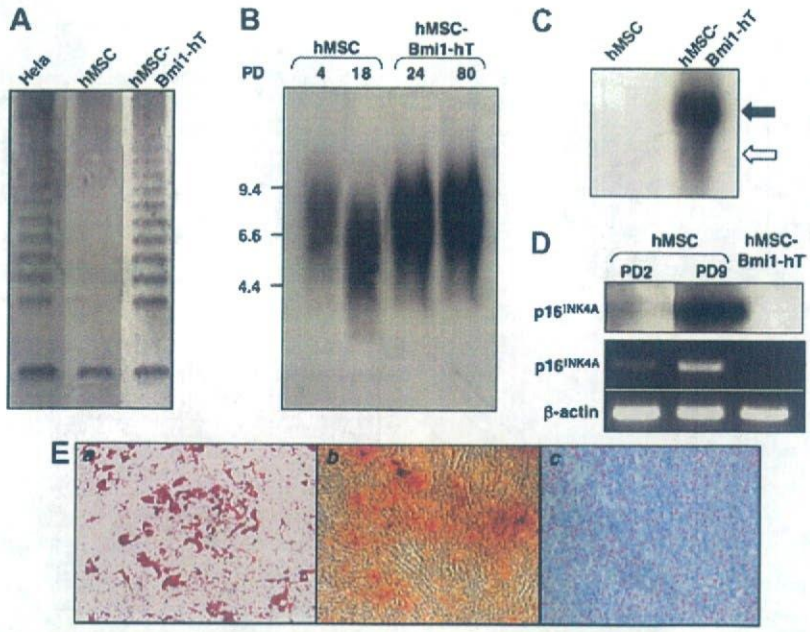

Fig. 1. Establishment of immortalized hMSC. (A) Telomerase activity of immortalized hMSC (hMSC-Bmi1-hT). (B) Telomere length of hMSC-Bmi1-hT in early and late passaged cells. (C) Expression of the exogenous Bmi1 gene. Closed and open arrows indicate the exogenous and endogenous Bmi1 gene, respectively. (D) Downregulation of $p16^{INK4A}$ expression at the mRNA and protein level in hMSC-Bmi-hT. (E) Potential of ihMSC to differentiate. Oil-Red-O, Alizarin red, and Alcian blue staining were performed after adipogenic, osteogenic, and chondrogenic induction, respectively.

differing in the potential to differentiate, as we previously found in a study of hMSC immortalized by the HPVE6/E7 genes [12]. Single cell cloning by the limited dilution method using 96-well culture plates was performed, and a total of 100 clones were isolated, and the potential of each clone to differentiate was analyzed. Five clones showed adipogenic, osteogenic, and chondrogenic differentiation potential, one of which was randomly selected for further study. The differentiation potential of this clone, hereafter called ihMSC, was stable even 24 months after cloning (Fig. 1E).

In vitro transformation of ihMSC by oncogenic H-ras^{Val12}

To test the potential of ihMSC to serve as cells for the screening of candidate oncogenes, the H-*ras*^{Val12} gene was introduced by a retroviral vector. The transduction of retroviral vectors expressing the oncogenic H-*ras*^{Val12} gene into ihMSC was independently performed in two experiments. Drug selection was started 48 h after the transduction, and cells were cultured and propagated until they grew stably. Polyclonal cell lines for each experiment were established, and designated ihMSC-*ras*-1 and ihMSC-*ras*-2. As a control, Mock-transfected cells were also established (ihMSC-Mock-1 and ihMSC-Mock-2). Expression of the exogenous H-*ras*^{Val12} gene was confirmed by Northern blotting (Supplementary Fig. 1). The karyotypic analysis of ihMSC-*ras*-1 showed that the dominant mode (39/50 metaphase) was (46, XY) with a marker chromosome (Supplementary Fig. 2). The doubling-time of the ihMSC-*ras* under standard (10% FBS) and serum-starved (1% FBS) conditions was 18.3 and 30.0 h, respectively, shorter than that of ihMSC (26.2 and 38.6 h). The anchorage-independent growth potential of ihMSC-*ras* was confirmed by performing a colony formation assay in soft agar (Fig. 2A). The motility of ihMSC-*ras* was significantly increased compared to that of ihMSC and ihMSC-Mock (Fig. 2B). Although the number of cells capable of invading the matrix was small, there was a significant difference between ihMSC-*ras* and ihMSC-Mock (Fig. 2C). The innoculation of ihMSC-*ras* into subcutaneous tissue in nude mice produced rapidly growing tumors with a frequency of 100% (Fig. 2D), the histological diagnosis being undifferentiated spindle cell tumors with no particular features (Fig. 2E). These results indicated that the introduction of the H-*ras*^{Val12} gene was able to completely transform ihMSC into undifferentiated sarcoma cells.

Induction of autophagy by oncogenic H-ras^{Val12}

There was a clear morphological difference val12 between the ihMSC and ihMSC-*ras* lines. Both ihMSC-*ras*-1 (Fig. 3A, b) and *ras*-2 (data not shown) had an abundance of cytosolic vacuoli, which were not found in ihMSC (Fig. 3A, a), ihMSC-Mock-1 or -2 (data not shown).

Transmission electron microscopic analysis revealed these vacuoli to be secondary lysosomes containing residual bodies (Fig. 3B), a feature of autophagy [13]. LC3 (microtubule-associated protein 1 light chain 3) is a human homologue of Atg8, which is a key molecule in the

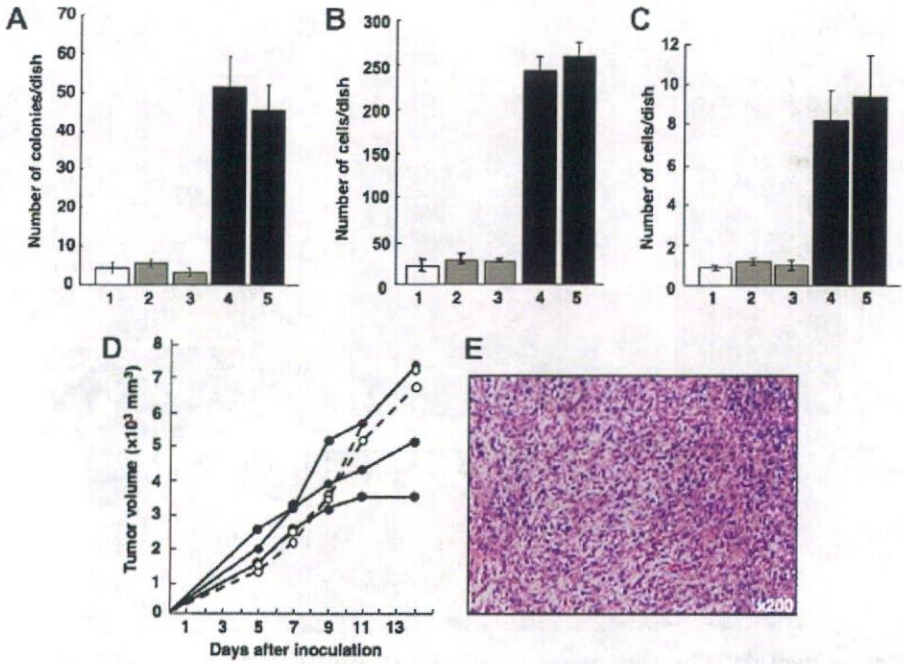

Fig. 2. Oncogenic property of ihMSC-*ras*. (A) Anchorage-independent growth. (B) Cell motility assay. (C) Cell invasion assay. Samples in each lane were: lane 1, ihMSC; lane 2, ihMSC-Mock-1; lane 3, ihMSC-Mock-2; lane 4, ihMSC-*ras*-1; and lane 5, ihMSC-*ras*-2. (D) Growth curve of *in vivo* tumors. Closed circles, ihMSC-*ras*-1 (three mice); open circles, ihMSC-*ras*-2 (two mice). (E) Histology of *in vivo* tumors produced by ihMSC-*ras*-1.

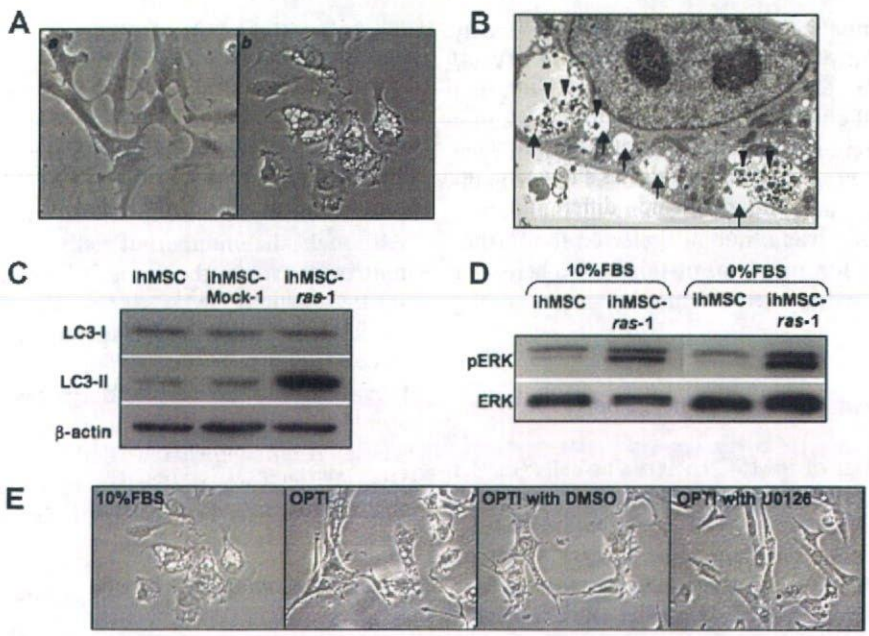

Fig. 3. Induction of autophagy by oncogenic H-*ras*^{Val12} in ihMSC. (A) Phase contrast micrographs of ihMSC (a), and ihMSC-*ras*-1 (b). (B) Transmission electron micrographs of ihMSC-*ras*-1. Arrows and arrowheads indicated secondary lysomes and residual bodies, respectively. (C) Western blot for LC3. Cell lysate was prepared from each cell line. (D) Expression of ERK1/2 in ihMSC lines. (E) Phase-contrast micrographs of ihMSC-*ras*-1 with or without treatment with U0126.

development of autophagosomes in yeast [14]. A C-terminal fragment of LC3 is cleaved immediately after synthesis, producing a cytosolic form known as LC3-I, and a subpopulation of LC3-I is further converted to an autophagosome-associating form, LC3-II [14]. Western blot analysis using the antibody against LC3 clearly showed the induction of LC3-II in ihMSC-*ras*-1 (Fig. 3C), and ihMSC-*ras*-2 (data not shown).